

Journal of Materials Chemistry A

Accepted Manuscript



This article can be cited before page numbers have been issued, to do this please use: J. Jiang, W. Liu, C. Wang, L. Zhang, H. Pan, W. Liu, J. Chen, D. Yang, Y. Xiang, K. Wang and X. Yao, *J. Mater. Chem. A*, 2019, DOI: 10.1039/C8TA11044A.



This is an Accepted Manuscript, which has been through the Royal Society of Chemistry peer review process and has been accepted for publication.

Accepted Manuscripts are published online shortly after acceptance, before technical editing, formatting and proof reading. Using this free service, authors can make their results available to the community, in citable form, before we publish the edited article. We will replace this Accepted Manuscript with the edited and formatted Advance Article as soon as it is available.

You can find more information about Accepted Manuscripts in the [author guidelines](#).

Please note that technical editing may introduce minor changes to the text and/or graphics, which may alter content. The journal's standard [Terms & Conditions](#) and the ethical guidelines, outlined in our [author and reviewer resource centre](#), still apply. In no event shall the Royal Society of Chemistry be held responsible for any errors or omissions in this Accepted Manuscript or any consequences arising from the use of any information it contains.

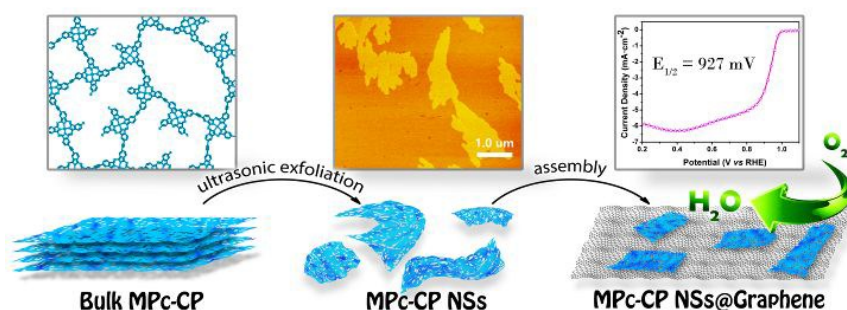
Exfoliation of Amorphous Phthalocyanine Conjugated Polymers into

View Article Online
DOI: 10.1039/C8TA11044A

Ultrathin Nanosheets for Highly Efficient Oxygen Reduction

Wenping Liu,^a Chiming Wang,^a Lijie Zhang,^d Houhe Pan,^a Wenbo Liu,^a Jun Chen,^c
Dongjiang Yang,^d Yanjuan Xiang,^e Kang Wang,^{*a,b} Jianzhuang Jiang^{*a} and Xiangdong
Yao^{*b}

Defects and disorders in the individual layers of ethynyl-linked phthalocyanine conjugated polymers (CPs) diminish interlayer π - π stacking interaction, which favors the exfoliation of these CPs into ultrathin 2D nanosheets (NSs) with high yield. In particular, the as-prepared bimetallic NSs could be further used to fabricate heterostructure with graphene NSs to boost the oxygen reduction in an alkaline medium.





Journal Name

ARTICLE

Exfoliation of Amorphous Phthalocyanine Conjugated Polymers into Ultrathin Nanosheets for Highly Efficient Oxygen Reduction †

Wenping Liu,^a Chiming Wang,^a Lijie Zhang,^d Houhe Pan,^a Wenbo Liu,^a Jun Chen,^c Dongjiang Yang,^d Yanjuan Xiang,^e Kang Wang,^{*a,b} Jianzhuang Jiang^{*a} and Xiangdong Yao^{*b}

Received 00th January 20xx,
Accepted 00th January 20xx

DOI: 10.1039/x0xx00000x

www.rsc.org/

It is a significant challenge to develop high-efficiency synthetic methodology to access fully conjugated 2D conjugated polymers (CPs)/covalent organic frameworks (COFs) nanosheets (NSs) that are of great application potential for electronics and energy. Herein, we report the exfoliation of a series of amorphous ethynyl-linked phthalocyanine (Pc) CPs (MPc-CPs, M = Fe, Co, Fe_{0.5}Co_{0.5}) into ultrathin MPc-CP NSs. Random coupling between the four regioisomers (with *D*_{4h}, *D*_{2h}, *C*_{2v} and *C*_s symmetry) of the two tetra-β-substituted phthalocyanine precursors endows the resulting phthalocyanine conjugated polymers MPc-CPs the intrinsic structural defects and disordered framework on individual layer. This in turn induces a diminished interlayer overlapping and a weakened interlayer π–π stacking interaction, rendering the possible exfoliation of MPc-CPs into ultrathin 2D NSs in a yield of over 50%. The direction observation by transmission electron microscopy (TEM) and atomic force microscopy (AFM) demonstrates that the ultrathin MPc-CP NSs possess a smooth surface with a uniform thickness of 1–3 nm and a lateral size of hundreds of nanometers. The as-prepared bimetallic Fe_{0.5}Co_{0.5}Pc-CP NSs was further used to fabricate heterostructure Fe_{0.5}Co_{0.5}Pc-CP NS@G with graphene NSs as an oxygen reduction reaction (ORR) catalyst, which exhibits an onset potential of 1006 mV and a half-wave potential of 927 mV in 0.1 M KOH, representing one of the best values in an alkaline medium. Moreover, the excellent ORR activity of the exfoliated tetrapyrrole-based conjugated NSs hybridized with graphene has also been demonstrated by the Zn-air battery device, showing an open circuit voltage of 1.34 V and a peak power density of ca. 180 mW cm⁻².

Introduction

Inspired by the discovery and prosperity of graphene, artificial two-dimensional (2D) organic conjugated layered materials with an extended π system, such as graphdiyne, 2D organic conjugated polymers (CPs), and 2D covalent organic frameworks (COFs),^{1–10} have received great research interest. Owing to the bottom-up approaches, the structures and components of such 2D polymers could be rationally designed and modulated at the atomic or molecular level, which will offer the desirable properties and functions with a wide range of applications in gas storage and separation,^{11,12} catalysis,^{13–16} sensors,^{17,18} and electronic devices.^{19–21} Recently, 2D conjugated CP/COF nanosheets (NSs) with a few

atomic layers have emerged as one new member in the 2D nanomaterials family and attracted increasing attention.^{22–26} Compared to the bulk CP/COF materials, 2D CP/COF nanosheets have unique superiorities. For instance, their larger surface area and more accessible active sites on the surfaces facilitate the contact with substrate molecules under lower diffusion barrier, and thus enhance the performance of 2D CP/COF nanosheets in catalysis and sensing applications.^{27–30} Additionally, the ultrathin structure would enable the formation of stable dispersions of the 2D CP/COF nanosheets, thus would enable large-area and low-cost liquid-deposition techniques, such as Quasi-Langmuir-Shäfe method, spin coating, or inkjet printing.^{31–34}

Generally, 2D CP/COF NSs are prepared by exfoliating their bulk counterparts by solvent-assisted liquid sonication,^{35,36} mechanical delamination,³⁷ self-exfoliation,³⁸ or sequential post-synthetic modification.³⁹ However, because of the strong interlayer π–π interactions, the exfoliation yield of the most obtained 2D CP/COF NSs is usually quite low. Recently, it has been reported that introduction of a cycloaddition reaction, twist, or flexible building units within the COF backbone is able to destroy/weaken the interlayer π–π interaction, leading to easier exfoliation of the bulk COF precursors into ultrathin NSs.^{30,40,41} However, the desired extended π conjugated structure was simultaneously destroyed/weakened by the aforementioned strategies, which may result in low electron transfer capability and thus limit their applications in electronics and energy-related fields. Therefore, new

^aBeijing Key Laboratory for Science and Application of Functional Molecular and Crystalline Materials, Department of Chemistry, University of Science and Technology Beijing, Beijing 100083, China. E-mail: jianzhuang@ustb.edu.cn, kangwang@ustb.edu.cn.

^bQueensland Micro- and Nanotechnology Centre, Griffith University, Nathan Campus QLD 4111, Australia. E-mail: x.yao@griffith.edu.au.

^cDepartment of Chemistry and Chemical Engineering, Henan Institute of Science and Technology, Xinxiang 453003, China.

^dCollaborative Innovation Center for Marine Biomass Fibers, Materials and Textiles of Shandong Province, College of Chemical and Environmental Engineering, Qingdao University, Qingdao 266071, China.

^eState Key Laboratory of Catalytic Material and Reaction Engineering, Research Institute of Petroleum Processing, SINOPEC, Beijing 100083, China.

† Electronic Supplementary Information (ESI) available: See DOI: 10.1039/x0xx00000x

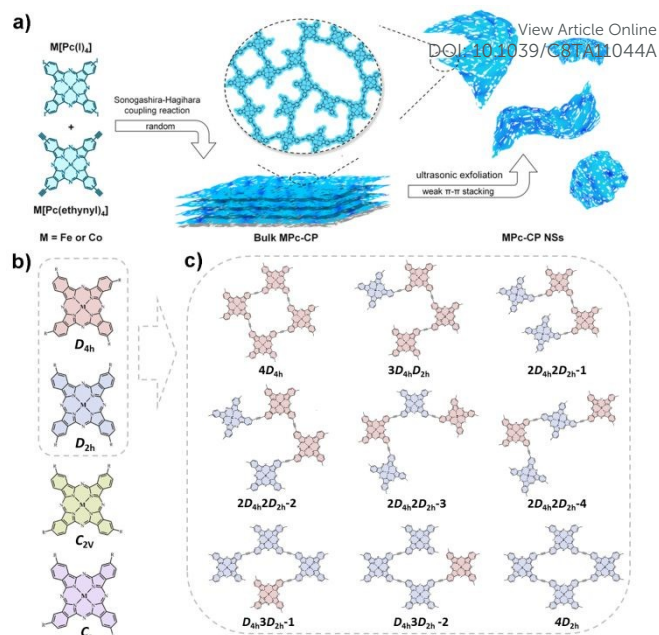
methodology still need to be established to develop high-efficiency synthetic methodology to access 2D CP/COF NSs.

Herein, we report a general approach to fabricate a series of ultrathin 2D CP NSs (MPc-CP NSs, $M = \text{Fe}_{0.5}\text{Co}_{0.5}$, Fe, and Co) with fully conjugated electronic structure, which was exfoliated from the ethynyl-linked phthalocyanine (Pc) CPs prepared from the phthalocyanine monomers, $\text{M}[\text{Pc}(\text{I})_4]$ and $\text{M}[\text{Pc}(\text{ethynyl})_4]$, through Sonagashira–Hagihara coupling reaction.⁴² Owing to that both the two tetra- β -substituted phthalocyanine precursors, $\text{M}[\text{Pc}(\text{I})_4]$ and $\text{M}[\text{Pc}(\text{ethynyl})_4]$, are composed of four regioisomers (with D_{4h} , D_{2h} , C_{2v} and C_s symmetry),⁴³ the as-synthesized CPs are of layered structure in which the layers are abundant with intrinsic structural defects and highly disordered framework nature. Such amorphous structure of the individual layer with defects enables the diminished interlayer overlapping area and weakened the interlayer π – π stacking interactions,^{44,45} rendering the easier and successful exfoliation of the bulk CP materials into ultrathin NSs with a high yield of over 50%. Meanwhile, hetero-assemblies of 2D nanolayers such as transition metal dichalcogenides/diseleniums,⁴⁶ layered double hydroxides,⁴⁷ and metal–organic frameworks⁴⁸ with various graphene NSs (including graphene, nitrogen doped graphene, and defective graphene) have been recently received increasing interest in fabricating versatile high performance electrocatalysts including oxygen reduction reaction (ORR), oxygen evolution reaction (OER), and hydrogen evolution reaction (HER) catalysts. The high activity is due to the combination of the highly exposed active centers presented on 2D nanolayers^{27–30} and high electron transfer capability of graphene NSs^{49–52} together with strong interaction between these components to reform the electronic distribution. Thanks to the ultrathin nature, the as-prepared bimetallic $\text{Fe}_{0.5}\text{Co}_{0.5}\text{Pc-CP}$ NSs was used to fabricate heterostructure $\text{Fe}_{0.5}\text{Co}_{0.5}\text{Pc-CP NS@G}$ with graphene NSs, which exhibits high ORR catalysis activity in an alkaline medium.

Results and Discussion

Synthesis and characterization of MPc-CP NSs.

Scheme 1a schematically illustrates the approach to fabricate ultrathin MPc-CP NSs. The bulk MPc-CP materials were prepared from corresponding $\text{M}[\text{Pc}(\text{I})_4]$ and $\text{M}[\text{Pc}(\text{ethynyl})_4]$ via Sonagashira–Hagihara coupling reaction according to previously reported procedure.⁴² Since both tetra- β -substituted phthalocyanine precursors, $\text{M}[\text{Pc}(\text{I})_4]$ and $\text{M}[\text{Pc}(\text{ethynyl})_4]$, are actually a mixture of four constitutional isomers (with D_{4h} , D_{2h} , C_{2v} and C_s symmetry) (Scheme 1b). Random coupling between the four $\text{M}[\text{Pc}(\text{I})_4]$ and $\text{M}[\text{Pc}(\text{ethynyl})_4]$ isomers leads to the formation of MPc-CPs with highly disordered individual layer. Scheme 1c shows a quadrilateral structure fabricated by four phthalocyanine molecules with D_{4h} or D_{2h} symmetry as an example to illustrate the disordered individual layer of MPc-CPs. As can be seen, nine structural models could be formed by random combination of four phthalocyanine molecules with D_{4h} or D_{2h} symmetry. The π – π interactions between the $4D_{4h}$ model with the nine structural models were also investigated by DFT calculations. As can be seen in Fig. S1 in ESI[†], the binding energy per phthalocyanine molecule between two different models



Scheme 1. (a) Synthesis of the phthalocyanine based CP NSs MPc-CP NSs ($M = \text{Fe}$, Co , and $\text{Fe}_{0.5}\text{Co}_{0.5}$). (b) The four kinds of isomers (with D_{4h} , D_{2h} , C_{2v} and C_s symmetry) for tetra- β -substituted phthalocyanines. (c) Nine quadrilateral structure models fabricated by four phthalocyanine molecules with D_{4h} or D_{2h} symmetry.

is 27–81% lower than that between two $4D_{4h}$ models, owing to the reduced overlapping area. These results suggest that the MPc-CP individual layers fabricated by more phthalocyanine molecules with four kinds of symmetry are completely disordered and amorphous. As a result, the interlayer overlapping area would be further diminished, which weakens the interlayer π – π stacking in the CPs, and in turn renders the possible exfoliation of the bulk MPc-CP materials into ultrathin 2D nanosheets by the subsequent solvent-assisted liquid sonication. With the bimetal counterparts $\text{Fe}_{0.5}\text{Co}_{0.5}\text{Pc-CP}$ NSs as representative, the yield of $\text{Fe}_{0.5}\text{Co}_{0.5}\text{Pc-CP}$ NSs could achieve *ca.* 36% after ultrasonic exfoliation for only 2 h in ethanol, with the maximum yield of *ca.* 51% achieved after 8 h (Fig. S2 in ESI[†]). The liquid sonication in other organic solvents such as acetone, tetrahydrofuran, and *N,N*-dimethylformamide also gave quite high yield of $\text{Fe}_{0.5}\text{Co}_{0.5}\text{Pc-CP}$ NSs (Fig. S2 in ESI[†]), suggesting the generality of the fabrication strategy.

The successful exfoliation of the bulk $\text{Fe}_{0.5}\text{Co}_{0.5}\text{Pc-CP}$ material into ultrathin $\text{Fe}_{0.5}\text{Co}_{0.5}\text{Pc-CP}$ NSs is firstly evidenced by the observation of a clear Tyndall effect when a green laser went through the suspension obtained after the ultrasonic exfoliation process (inset in Fig. 1a). Transmission electron microscopy (TEM) image reveals a graphene-like structure of transparent $\text{Fe}_{0.5}\text{Co}_{0.5}\text{Pc-CP}$ NSs with a lateral size of several hundred nanometers (Fig. 1a), further confirming the formation of ultrathin $\text{Fe}_{0.5}\text{Co}_{0.5}\text{Pc-CP}$ NSs. The thickness of the $\text{Fe}_{0.5}\text{Co}_{0.5}\text{Pc-CP}$ NSs was measured by atomic force microscopy (AFM). It can be seen in Fig. 1b and 1c that the $\text{Fe}_{0.5}\text{Co}_{0.5}\text{Pc-CP}$ NSs possess a smooth surface with a uniform thickness of 1.05 ± 0.05 nm, corresponding to three layers.

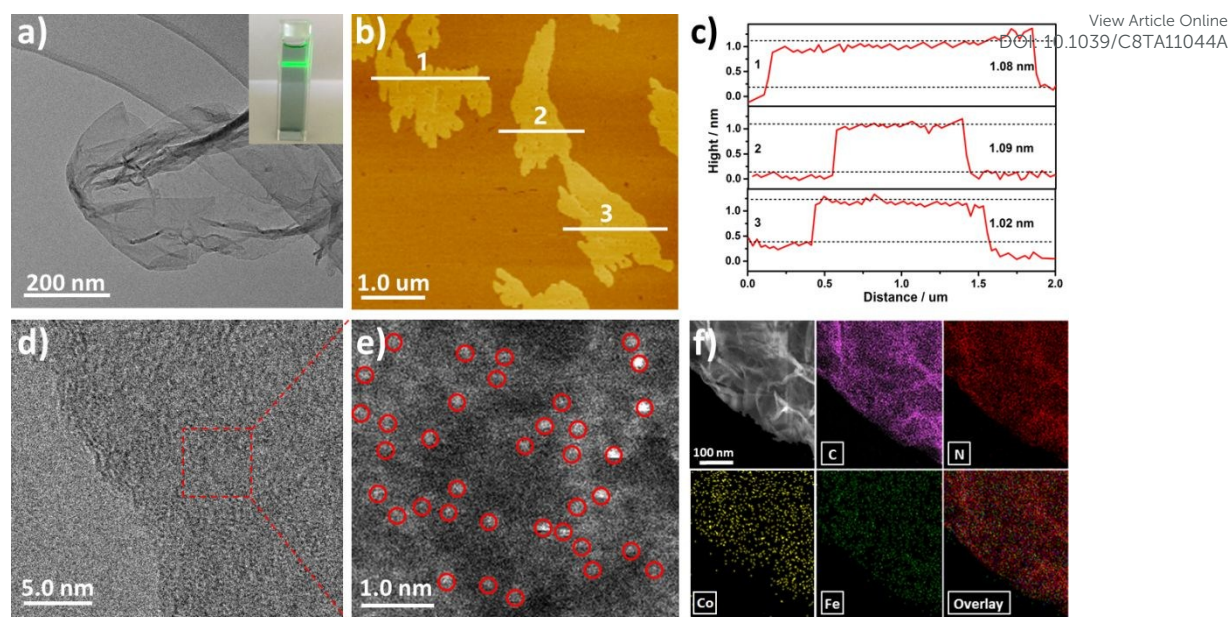


Fig. 1 (a) TEM image of $\text{Fe}_{0.5}\text{Co}_{0.5}\text{Pc-CP}$ NSs. Inset: Photograph of the Tyndall effect of the $\text{Fe}_{0.5}\text{Co}_{0.5}\text{Pc-CP}$ NSs suspension. (b) AFM image and (c) the corresponding height profiles of $\text{Fe}_{0.5}\text{Co}_{0.5}\text{Pc-CP}$ NSs. (d) AC STEM image and (e) enlarged image of the $\text{Fe}_{0.5}\text{Co}_{0.5}\text{Pc-CP}$ NSs. (single Fe/Co atoms are highlighted by red circles). (f) HAADF-STEM image and elemental mapping of C, N, Co, and Fe of the $\text{Fe}_{0.5}\text{Co}_{0.5}\text{Pc-CP}$ NSs.

Nevertheless, no obvious lattice fringes are observed in aberration-corrected scanning transmission electron microscopy (AC STEM) images (Fig. 1d), which indicates the amorphous nature of the CP individual layers originated from the less symmetrical isomers in $\text{Fe}[\text{Pc}(\text{I})_4]$ and $\text{Co}[\text{Pc}(\text{ethynyl})_4]$. This is also supported by the fact that the selected area electron diffraction (SAED) pattern of the $\text{Fe}_{0.5}\text{Co}_{0.5}\text{Pc-CP}$ NSs shows broad halo rings (Fig. S3 in ESI†). Moreover, from aberration-corrected high-angle annular dark-field STEM (AC HAADF-STEM) presented in Fig. 1e, bright dots (highlighted by red circles) are observed, which are corresponding to single Fe/Co atoms located in N_4 -coordination sites of phthalocyanine ligands. In particular, the random dispersion of these Fe/Co atoms also suggests the disordered framework of the $\text{Fe}_{0.5}\text{Co}_{0.5}\text{Pc-CP}$ NSs. Energy dispersive spectroscopy (EDS) and X-ray photoelectron spectra (XPS) results indicate that the $\text{Fe}_{0.5}\text{Co}_{0.5}\text{Pc-CP}$ NSs are composed of C, N, O, I, Fe and Co, in accordance with the composition of bulk $\text{Fe}_{0.5}\text{Co}_{0.5}\text{Pc-CP}$ material (Fig. S4 in ESI†).⁴⁹ The element mapping verifies the homogenous surface distribution of Co, Fe, C, and N throughout the whole $\text{Fe}_{0.5}\text{Co}_{0.5}\text{Pc-CP}$ NSs (Fig. 1f). These analysis results, together with almost the same Fourier transform infrared, XPS, and solid-state UV-vis diffuse reflectance spectra between bulk $\text{Fe}_{0.5}\text{Co}_{0.5}\text{Pc-CP}$ and $\text{Fe}_{0.5}\text{Co}_{0.5}\text{Pc-CP}$ NSs, demonstrate that the chemical composition and bonding modes remain intact after the ultrasonic exfoliation (Fig. S5 in ESI†). In addition, the Brunauer-Emmett-Teller (BET) surface area of $\text{Fe}_{0.5}\text{Co}_{0.5}\text{Pc-CP}$ NSs is $80 \text{ m}^2 \text{ g}^{-1}$ calculated from the N_2 sorption isotherm at 77K, attributed to the mesopores formed by aggregation of nanosheets (Fig. S5 in ESI†). This is significantly larger than that of the bulk $\text{Fe}_{0.5}\text{Co}_{0.5}\text{Pc-CP}$ ($17 \text{ m}^2 \text{ g}^{-1}$), suggesting more active metal centers are exposed on the ultrathin nanosheets. The individual metal counterparts, FePc-CP NSs and CoPc-CP NSs,

were also prepared under the same conditions with a yield of 42 and 60%, respectively (Fig. S6–S9 in ESI†), which show similar shape, thickness (1.0 nm for CoPc-CP NSs and 3.2 nm for FePc-CP NSs), and surface area to the $\text{Fe}_{0.5}\text{Co}_{0.5}\text{Pc-CP}$ NSs. Additionally, the diyne linked Pc conjugated polymer CoPc-CP-2 fabricated from the alkyne–alkyne homocoupling reaction of $\text{Co}[\text{Pc}(\text{ethynyl})_4]$ could be also exfoliated into ultrathin NSs in the yield ca. 40% (Fig. S10 in ESI†). All above also demonstrate the generality of the present fabrication strategy to exfoliate CPs to ultrathin conjugated polymer NSs.

It is worth noting again that the successful exfoliation of these Pc-based CP materials to 2D ultrathin NSs by liquid sonication origin the weak interlayer interactions in bulk Pc-based CP materials, due to their intrinsic defected and highly disordered 2D networks. On the other hand, if the CPs are with order stacking structure and less defects, it is very hard to exfoliate them to ultrathin NSs. For example, a 2D layered Pc-based CP, denoted as FePc-CP-3 , is synthesized from the reaction between 1,2,4,5-benzenetetraniitrile and FeCl_2 (see the ESI† for details).^{53,54} The ordered AA stacking crystal structure of FePc-CP-3 was confirmed by Powder X-ray diffraction (PXRD) and HRTEM (Fig. S11b and S11c in ESI†). In contrast to MPc-CPs and CoPc-CP-2 , only few bulk FePc-CP-3 material (<5%) was exfoliated into NSs with the thickness in wide range after ultrasonic exfoliation for 8 h in ethanol, (Fig. S11d in ESI†), because of the intense interlayer π – π interaction.

Preparation of $\text{Fe}_{0.5}\text{Co}_{0.5}\text{Pc-CP}$ NS@G heterostructure.

It is previously reported that the bulk $\text{Fe}_{0.5}\text{Co}_{0.5}\text{Pc-CP}$ material exhibit good ORR activity owing to the synergetic effect between the proximate Fe and Co ions in the conjugated polymer.⁴²

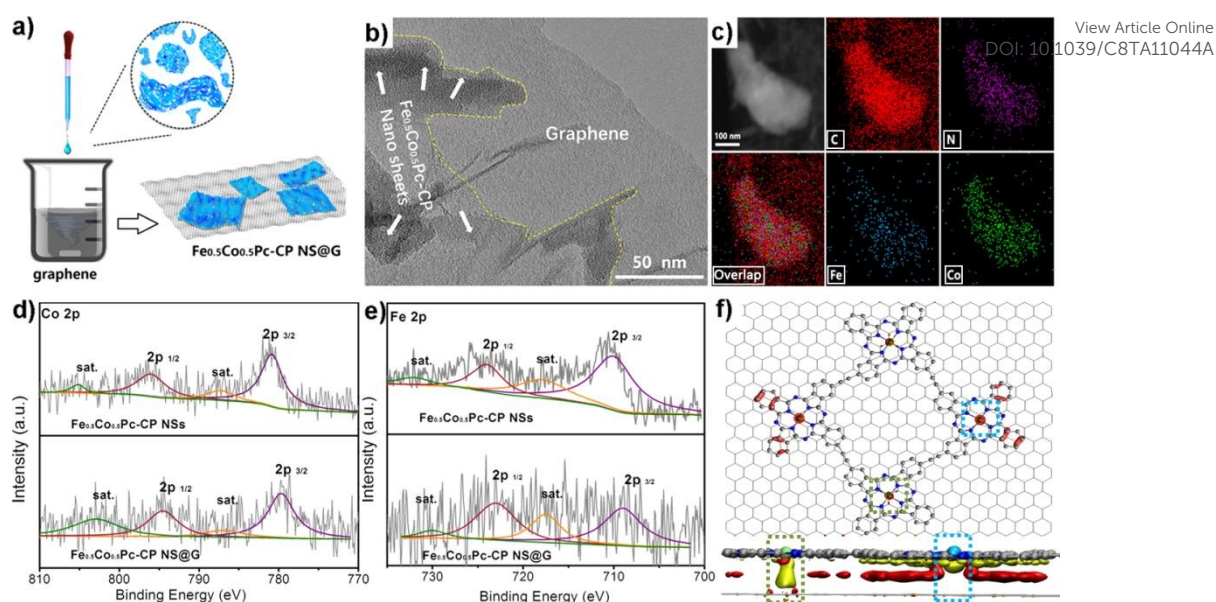


Fig. 2 (a) Schematic illustration of synthetic Fe_{0.5}Co_{0.5}Pc-CP NS@G. (b) TEM image of Fe_{0.5}Co_{0.5}Pc-CP NS@G. (c) HAADF-STEM image and corresponding elemental mapping of C, N, Co, and Fe. (d, e) XPS spectra of Fe 2p and Co 2p of Fe_{0.5}Co_{0.5}Pc-CP NSs and Fe_{0.5}Co_{0.5}Pc-CP NS@G. (f) The top and side views of charge density difference plot for the interfaces between Fe_{0.5}Co_{0.5}Pc-CP NS and graphene. Yellow and red isosurfaces indicate charge accumulation and depletion, respectively, with an isosurface value of 0.002 e Å⁻³. For clarity, the graphene and Fe_{0.5}Co_{0.5}Pc-CP NS are shown in stick and ball-and-stick models, respectively. Gray, blue, ice blue, and light green balls represent C, N, Fe, and Co atoms in Fe_{0.5}Co_{0.5}Pc-CP NS, respectively.

Normally, the ultrathin NSs are more active than the bulk counterpart attributed to the more exposed catalytic sites and easier mass transportation. Accordingly, it is reasonable to hypothesize that the ORR activity can be significantly improved if coupling the ultrathin Fe_{0.5}Co_{0.5}Pc-CP NSs and graphene to fabricate heterostructure Fe_{0.5}Co_{0.5}Pc-CP NS@G. The synthesis strategy of Fe_{0.5}Co_{0.5}Pc-CP NS@G is shown in Fig. 2a. Owing to the conjugated structure of both components, Fe_{0.5}Co_{0.5}Pc-CP NSs and graphene NSs were easily hybridized together depending on effective interlayer π - π interactions. It is directly observed by TEM (Fig. 2b) that the Fe_{0.5}Co_{0.5}Pc-CP NSs were assembled on the surface of graphene NSs. EDS mapping analysis indicates a coincided distribution of Fe, Co, and N throughout the exfoliated Fe_{0.5}Co_{0.5}Pc-CP NSs on graphene NSs (Fig. 2b). Furthermore, XPS was also conducted to investigate the as-prepared heterostructure. As can be seen in Fig. S12, the XPS full survey of Fe_{0.5}Co_{0.5}Pc-CP NS@G reveals the presence of C, N, O, I, Fe, and Co elements, well consistent with the EDS results (Fig. S13 in ESI[†]). In the Fe 2p spectrum, two peaks of the Fe 2p_{3/2} and Fe 2p_{1/2} were observed at 709.0 and 722.9 eV of Fe_{0.5}Co_{0.5}Pc-CP NS@G (Fig. 2d), while the Co 2p spectrum displayed the two peaks of Co 2p_{3/2} and Co 2p_{1/2} at 779.7 and 794.5 eV (Fig. 2e), respectively. Interestingly, compared to the Fe_{0.5}Co_{0.5}Pc-CP NSs, the peaks of Fe 2p and Co 2p of Fe_{0.5}Co_{0.5}Pc-CP NS@G shift to the lower energy, indicating a strong interaction between Fe_{0.5}Co_{0.5}Pc-CP NSs and graphene NSs in the as-prepared heterostructure. Generally, the decrease in binding energy reveals an enhanced electron screening effect because of the increase in electron density. These results suggest the charge transfer between the two components in the interface of Fe_{0.5}Co_{0.5}Pc-CP NS@G, resulting in the electron accumulation at the

metal sites in Fe_{0.5}Co_{0.5}Pc-CP NSs. To further demonstrate this point, density functional theory (DFT) calculations were carried out at the level of PBE/Lanl2DZ/3-21G (for C, H, N atoms) using Gaussian 09 D.01.⁵⁵⁻⁵⁸ Fig. 2f shows the geometry of the fully relaxed Fe_{0.5}Co_{0.5}Pc-CP NS@G composite as well as the charge density differences. As shown, the electrons tended to redistribute around the metal sites after assembling the Fe_{0.5}Co_{0.5}Pc-CP NSs and graphene NSs together, which favors to bind O₂ molecules. This, in combination with the highly exposed active centers, suggests the optimized ORR performance of Fe_{0.5}Co_{0.5}Pc-CP NS@G.

ORR electrocatalytic activity.

The ORR property of Fe_{0.5}Co_{0.5}Pc-CP NS@G was evaluated by steady-state linear sweep voltammetry (LSV) on a rotating disk electrode (RDE) with the rotation speed of 1600 rpm in O₂-saturated 0.1 M KOH solution. For purpose of illustrating the key factors that contributed to the ORR performance of Fe_{0.5}Co_{0.5}Pc-CP NS@G, the electrocatalytic properties of heterostructures with different contents were measured (Fig. S14 in ESI[†]). As can be seen, Fe_{0.5}Co_{0.5}Pc-CP@G with the ratio between Fe_{0.5}Co_{0.5}Pc-CP NS and G of 2:1 exhibits the best catalytic activity. For comparison, the LSV curves of the composite of bulk Fe_{0.5}Co_{0.5}Pc-CP and graphene (2:1) (denoted as Fe_{0.5}Co_{0.5}Pc-CP&G) as well as the commercial Pt/C (20 wt%) were also recorded. As shown in Fig. 3a, Fe_{0.5}Co_{0.5}Pc-CP NS@G (the ratio between Fe_{0.5}Co_{0.5}Pc-CP NS and G is 2:1) exhibited an E_{onset} of 1006 mV vs RHE and an $E_{1/2}$ of 927 mV vs RHE, obviously superior to Fe_{0.5}Co_{0.5}Pc-CP&G (E_{onset} = 954 mV vs RHE and $E_{1/2}$ = 855 mV vs RHE). Remarkably, with similar onset potential, the $E_{1/2}$ of

$\text{Fe}_{0.5}\text{Co}_{0.5}\text{Pc-CP NS@G}$ is 83 mV more positive than that of the commercial Pt/C (20 wt%) ($E_{1/2} = 844$ mV vs RHE), outperforming most of the state-of-the-art ORR catalysts reported to date in an alkaline medium (see Table S1 in ESI†). The electrochemical active surface areas (ECSAs) and mass activity of $\text{Fe}_{0.5}\text{Co}_{0.5}\text{Pc-CP NS@G}$ and $\text{Fe}_{0.5}\text{Co}_{0.5}\text{Pc-CP@G}$ were also determined to further evaluate their performance. $\text{Fe}_{0.5}\text{Co}_{0.5}\text{Pc-CP NS@G}$ shows an ECSA of 159 cm^2 , significantly higher than that of $\text{Fe}_{0.5}\text{Co}_{0.5}\text{Pc-CP@G}$, 90 cm^2 (Fig. S15 in ESI†). The mass activity and turnover frequency of $\text{Fe}_{0.5}\text{Co}_{0.5}\text{Pc-CP NS@G}$ are determined to be 18.9 A/g and 42.5 s^{-1} at 0.9 V vs RHE (Fig. 3b), respectively, which are significantly higher than those of $\text{Fe}_{0.5}\text{Co}_{0.5}\text{Pc-CP@G}$ (11.1 A/g and 28.7 s^{-1}) and Pt/C (20 wt%) (7.5 A/g and 1.2 s^{-1}), and comparable with the best values for Pt-free catalysts reported so far.^{42,59–66} These results coincide well with our expectation that $\text{Fe}_{0.5}\text{Co}_{0.5}\text{Pc-CP NS@G}$ would show an enhanced ORR performance. The high ORR catalytic activity of $\text{Fe}_{0.5}\text{Co}_{0.5}\text{Pc-CP NS@G}$ was further revealed by the catalytic selectivity. The electron transfer number n of $\text{Fe}_{0.5}\text{Co}_{0.5}\text{Pc-CP NS@G}$, analysed based on the RDE measurements at different rotating speeds according to the Koutecký–Levich (K–L) equation, was *ca.* 4

at $0.4\text{--}0.7 \text{ V}$ vs RHE (Fig. 3c), indicating the ORR at the $\text{Fe}_{0.5}\text{Co}_{0.5}\text{Pc-CP NS@G}$ electrode proceeds via a $4e^-$ reduction pathway. The rotation ring-disk electrode (RRDE) measurements were further carried out to determine the electron transfer number n and monitor the generation of peroxide. It can be seen in Fig. 3d, n was calculated to be over 3.9 at $0.3\text{--}0.9 \text{ V}$ vs RHE with peroxide yield below 5%, confirming the $4e^-$ reduction pathway over $\text{Fe}_{0.5}\text{Co}_{0.5}\text{Pc-CP NS@G}$. Besides the high ORR activity, the amperometric *i*-t test revealed that the stability of $\text{Fe}_{0.5}\text{Co}_{0.5}\text{Pc-CP NS@G}$ is superior to Pt/C (20 wt%) (Fig. 3e). Furthermore, the XPS spectra of $\text{Fe}_{0.5}\text{Co}_{0.5}\text{Pc-CP NS@G}$ were recorded after the *i*-t test, which was almost unchanged, confirming its high stability (see Fig. S16 in ESI†). Moreover, $\text{Fe}_{0.5}\text{Co}_{0.5}\text{Pc-CP NS@G}$ exhibit more excellent tolerance for methanol compared to Pt/C (20 wt%) (Fig. 3f). These results endow $\text{Fe}_{0.5}\text{Co}_{0.5}\text{Pc-CP NS@G}$ an alternative cathode catalyst in methanol fuel cells and metal-air batteries.

Zn–air batteries.

Inspired by the notable half-cell performance of $\text{Fe}_{0.5}\text{Co}_{0.5}\text{Pc-CP NS@G}$ in the ORR, this catalyst was further utilized as a cathode to evaluate the full-cell application in the Zn–air batteries under practical conditions (Fig. 4a). For the purpose of comparison, Pt/C (20 wt%) was also integrated into a Zn–air battery. As shown in Fig. 4b, the discharge polarization and power density plots of the $\text{Fe}_{0.5}\text{Co}_{0.5}\text{Pc-CP NS@G}$ Zn–air battery show an open circuit voltage of 1.34 V and a maximum power density of *ca.* 180 mW cm^{-2} at a current density of 283 mA cm^{-2} , which are better than those of the Pt/C (20 wt%) (with the open circuit voltage of 1.33 V and the peak power density of *ca.* 152 mW cm^{-2}). In addition, $\text{Fe}_{0.5}\text{Co}_{0.5}\text{Pc-CP NS@G}$ Zn–air battery exhibit stable discharge voltage at a current density of 10 mA cm^{-2} , comparable to that of the Pt/C (20 wt%) (Fig. 4c). To further broaden the application of $\text{Fe}_{0.5}\text{Co}_{0.5}\text{Pc-CP NS@G}$, a rechargeable Zn–air battery was fabricated with the mixture of $\text{Fe}_{0.5}\text{Co}_{0.5}\text{Pc-CP NS@G}$ and RuO (a benchmark electrocatalyst for the oxygen evolution reaction) (1:1) as the cathode. This rechargeable Zn–air battery exhibits the very similar discharge polarization and power density plots as the $\text{Fe}_{0.5}\text{Co}_{0.5}\text{Pc-CP NS@G}$ Zn–air battery (Fig. 4b), clearly indicating the dominant contribution of $\text{Fe}_{0.5}\text{Co}_{0.5}\text{Pc-CP NS@G}$ to the ORR activity in the cathode of the rechargeable Zn–air battery. Moreover, long-term cycling tests at current densities of 5 and 10 mA cm^{-1} reveal the lack of obvious change for discharge voltage over 200 cycles (Fig. 4d). Additionally, two rechargeable Zn–air batteries in series could provide an enough high open circuit voltage to power a light-emitting diode (LED) light with a rated voltage of $\approx 2 \text{ V}$ (Fig. 4e). These results disclose the great potential of the $\text{Fe}_{0.5}\text{Co}_{0.5}\text{Pc-CP NS@G}$ composite in the Zn–air batteries applications.

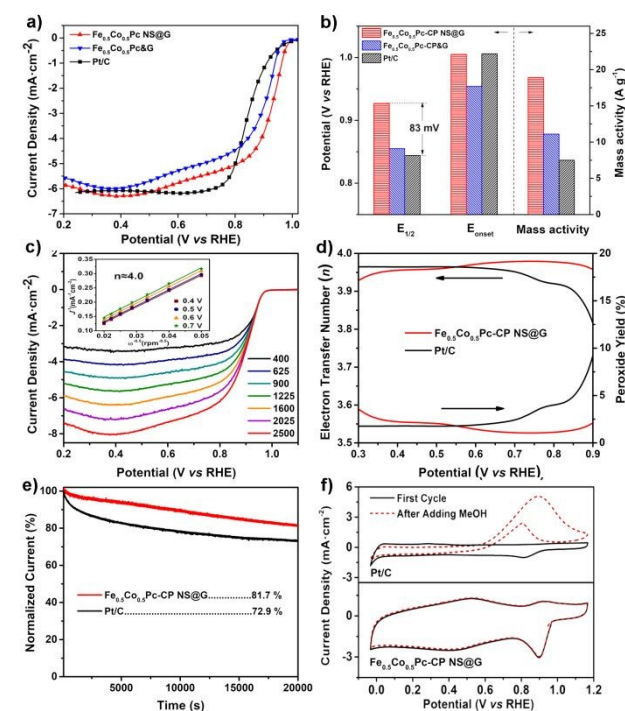


Fig. 3 (a) LSV curves of $\text{Fe}_{0.5}\text{Co}_{0.5}\text{Pc-CP NS@G}$, $\text{Fe}_{0.5}\text{Co}_{0.5}\text{Pc-CP@G}$, and Pt/C (20%) measured in O_2 -saturated 0.1 M KOH solution. (b) Onset potential, half-wave potential and mass activity comparisons of $\text{Fe}_{0.5}\text{Co}_{0.5}\text{Pc-CP NS@G}$, $\text{Fe}_{0.5}\text{Co}_{0.5}\text{Pc-CP@G}$ and Pt/C (20%). (c) LSV curves at different rotation speeds of $\text{Fe}_{0.5}\text{Co}_{0.5}\text{Pc-CP NS@G}$. The inset shows K–L plots. (d) H_2O_2 yield and electron transfer number of $\text{Fe}_{0.5}\text{Co}_{0.5}\text{Pc-CP@G}$ and Pt/C (20%). (e) Amperometric *i*-t curves of $\text{Fe}_{0.5}\text{Co}_{0.5}\text{Pc-CP NS@G}$ and Pt/C (20%) under the rotation speed of 1600 rpm . (f) Methanol tolerance test for $\text{Fe}_{0.5}\text{Co}_{0.5}\text{Pc-CP NS@G}$ and Pt/C (20%).

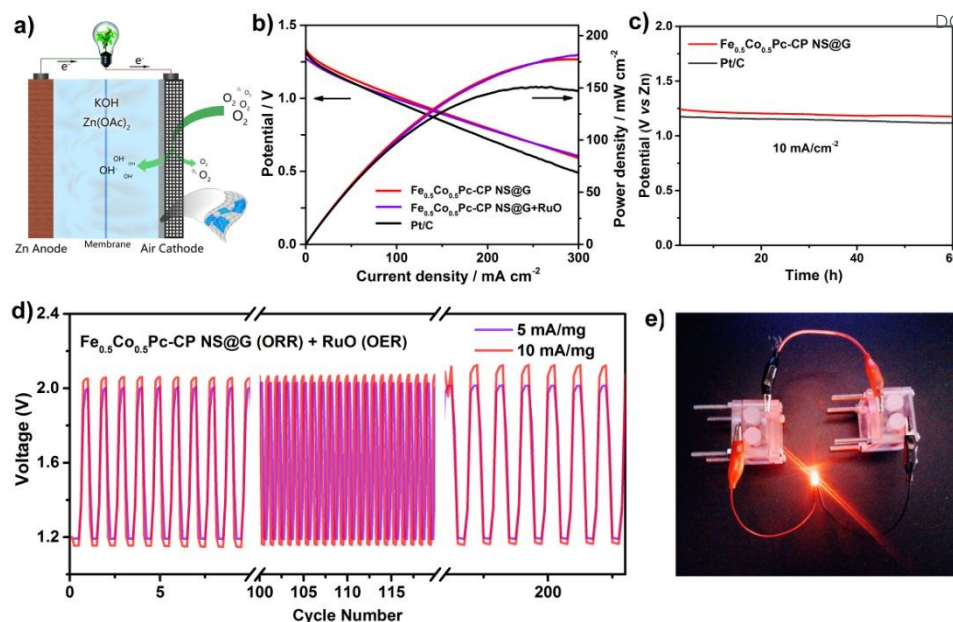


Fig. 4 (a) Schematic of the Zn–air battery. (b) The discharge polarization plots and power density curves of the Zn–air batteries. (c) Discharge plots of the Zn–air batteries with Fe_{0.5}Co_{0.5}Pc-CP NS@G as well as commercial Pt/C (20%) as cathode catalysts at a current density of 10 mA cm⁻². (d) The discharge and charge voltage profiles of the Zn–air batteries with the mixture of Fe_{0.5}Co_{0.5}Pc-CP NS@G and RuO (1:1) as the cathode at current densities of 5 and 10 mA mg⁻¹. (e) Photographs of a LED light (≈ 2 V) powered by two zinc–air batteries with the mixture of Fe_{0.5}Co_{0.5}Pc-CP NS@G and RuO as the cathode in series.

Conclusions

We report the efficient exfoliation of a series of conjugated ultrathin MPC-CP NSs (M = Fe, Co, Fe_{0.5}Co_{0.5}) from their bulk counterparts, owing to the introduction of the defects and disorders into the individual layers, which enable diminished interlayer overlapping and weakened interlayer π – π stacking. The ultrathin MPC-CP NSs possess a smooth surface with a uniform thickness and a lateral size of several hundred nanometers. The as-prepared bimetallic Fe_{0.5}Co_{0.5}Pc-CP NSs can be used to fabricate heterostructure Fe_{0.5}Co_{0.5}Pc-CP NS@G with graphene NSs as a high-performance ORR catalysts with an onset potential of 1006 mV and a half-wave potential of 927 mV in 0.1 M KOH, outperforming most of the state-of-the-art ORR catalysts reported so far in an alkaline medium. Its excellent ORR activity has also been demonstrated by the good performance of the Zn–air battery device, with an open circuit voltage of 1.34 V and a peak power density of ≈ 180 mW cm⁻². This work is surely helpful for further design and synthesis of other ultrathin 2D CP/COF NSs with tunable conjugated electronic and geometric structure, which might have various promising applications in electronics and energy-related fields.

Experimental Section

General Remarks

All reagents and solvents were reagent grade and used as received. Fe_{0.5}Co_{0.5}Pc-CP, CoPc-CP, FePc-CP, and CoPc-CP-2 were synthesized by using reported procedures.⁴²

Preparation of Fe_{0.5}Co_{0.5}Pc-CP NSs, FePc-CP NSs, and CoPc-CP NSs

The NSs were obtained by exfoliation of bulk MPC-CP materials *via* a simple sonication procedure. In a typical experiment, Fe_{0.5}Co_{0.5}Pc-CP powder (20 mg) was dispersed in ethanol (60 mL). The suspension was then sonicated in an ultrasonication bath (KQ-500DE, 40 kHz, 500W) for 8 h under room temperature. The resulting suspension was centrifuged at 2000 rpm for 5 min to remove the unexfoliated bulk Fe_{0.5}Co_{0.5}Pc-CP. The yield is calculated by measuring the remaining weight of collected unexfoliated bulk Fe_{0.5}Co_{0.5}Pc-CP and compared to the weight of original crystals before sonication. As a result, the measured yield is 51%. FePc-CP NSs, CoPc-CP NSs, and CoPc-CP-2 NSs were prepared by the same procedure with the yield of 42%, 60%, and 40%, respectively.

Preparation of Fe_{0.5}Co_{0.5}Pc-CP NS@G

Typically, a designed volume (2.0 mg mL⁻¹) of the exfoliated Fe_{0.5}Co_{0.5}Pc-CP NSs was added drop by drop into graphene NSs suspension with concentration of 1.0 mg mL⁻¹ under continuous stirring for 8 h at 70°C. The flocculated product was separated by centrifugation. The weight ratios of Fe_{0.5}Co_{0.5}Pc-CP NS and G were controlled as 1:1, 2:1, 4:1, and 8:1.

Preparation of Fe_{0.5}Co_{0.5}Pc-CP&G

Fe_{0.5}Co_{0.5}Pc-CP&G was prepared by the same procedure of Fe_{0.5}Co_{0.5}Pc-CP NS@G with the Fe_{0.5}Co_{0.5}Pc-CP NSs replaced by bulk Fe_{0.5}Co_{0.5}Pc-CP.

Acknowledgements

Financial support from the Natural Science Foundation of China (Nos. 21631003, 21671017, and 21871024), the Fundamental Research Funds for the Central Universities (No. FRF-BD-17-016A), and University of Science and Technology Beijing is gratefully acknowledged.

References

- S.-Y. Ding and W. Wang, *Chem. Soc. Rev.*, 2013, **20**, 548-568.
- H. Furukawa and O. M. Yaghi, *J. Am. Chem. Soc.*, 2009, **131**, 8875-8883.
- Y. Xu, S. Jin, H. Xu, A. Nagai and D. Jiang, *Chem. Soc. Rev.*, 2013, **42**, 8012-8031.
- X. Ding, B. Han, *Angew. Chem., Int. Ed.*, 2015, **54**, 6536-6539.
- K. Wang, D. Qi, Y. Li, T. Wang, H. Liu and J. Jiang, *Coord. Chem. Rev.*, 2017, DOI: 10.1016/j.ccr.2017.08.023.
- G. Li, Y. Li, H. Liu, Y. Guo, Y. Li and D. Zhu, *Chem. Commun.*, 2010, **46**, 3256-3258.
- Y. Xue, Y. Li, J. Zhang, Z. Liu and Y. Zhao, *Sci. China: Chem.*, 2018, **61**, 765-786.
- C. Huang, Y. Li, N. Wang, Y. Xue, Z. Zuo, H. Liu and Y. Li, *Chem. Rev.*, 2018, **118**, 7744-7803.
- H. Yu, Y. Xue, L. Hui, C. Zhang, Y. Li, Z. Zuo, Y. Zhao, Z. Li and Y. Li, *Adv. Mater.*, 2018, **30**, 1707082.
- Y. Xue, B. Huang, Y. Yi, Y. Guo, Z. Zuo, Y. Li, Z. Jia, H. Liu and Y. Li, *Nat. Commun.*, 2018, **9**, 1-10.
- Z. Kang, Y. Peng, Y. Qian, D. Yuan, M. A. Addicoat, T. Heine, Z. Hu, L. Tee, Z. Guo and D. Zhao, *Chem. Mater.*, 2016, **28**, 1277-1285.
- S. Keskin, *J. Phys. Chem. C*, 2012, **116**, 1772-1779.
- R. Dong, Z. Zheng, X. Zhu, J. Zhang, X. Feng, M. Pfeiffermann and H. Liang, *Angew. Chem., Int. Ed.*, 2015, **54**, 12058-12063.
- Z. Xiang, D. Cao, L. Huang, J. Shui, M. Wang and L. Dai, *Adv. Mater.*, 2014, **26**, 3315-3320.
- J. Zhang, F. Guo and X. Wang, *Adv. Funct. Mater.*, 2013, **23**, 3008-3014.
- Q. Xu, Y. Tang, X. Zhang, Y. Oshima, Q. H. Chen and D. Jiang, *Adv. Mater.*, 2018, **30**, 1706330.
- M. Zhang, G. Feng, Z. Song, Y.-P. Zhou, H.-Y. Chao, D. Yuan, T. T. Y. Tan, Z. Guo, Z. Hu, B. Z. Tang, B. Liu and D. Zhao, *J. Am. Chem. Soc.*, 2014, **136**, 7241-7244.
- H. Xu, J. Gao, X. Qian, J. Wang, H. He, Y. Cui, Y. Yang, Z. Wang and G. Qian, *J. Mater. Chem. A*, 2016, **4**, 10900-10905.
- Y. Gao, H. L. Yip, K. S. Chen, K. M. O'Malley, O. Acton, Y. Sun, G. Ting, H. Z. Chen and A. K. Y. Jen, *Adv. Mater.*, 2011, **23**, 1903-1908.
- J. W. Colson, A. R. Woll, A. Mukherjee, M. P. Levendorf, E. L. Spitler, V. B. Shields, M. G. Spencer, J. Park and W. R. Dichtel, *Science*, 2011, **332**, 228-231.
- J. Dugay, M. Gimenez-Marques, T. Kozlova, H. W. Zandbergen, E. Coronado and H. S. J. van der Zant, *Adv. Mater.*, 2015, **27**, 1288-1293.
- S. Zhao, Y. Wang, J. Dong, C.-T. He, H. Yin, P. An, K. Zhao, X. Zhang, C. Gao, L. Zhang, J. Lv, J. Wang, J. Zhang, A. M. Khattak, N. Ali Khan, Z. Wei, J. Zhang, S. Liu, H. Zhao and Z. Tang, *Nat. Energy*, 2016, **1**, 16184.
- Y. Ma, B. Li and S. Yang, *Mater. Chem. Front.*, 2018, **2**, 456-467.
- M. Osada and T. Sasaki, *Adv. Mater.*, 2012, **24**, 210-228.
- X. Huang, C. Tan, Z. Yin and H. Zhang, *Adv. Mater.*, 2014, **26**, 2185-2204.
- H. Sahabudeen, H. Y. Qi, B. A. Glatz, D. Tranca, R. H. Dong, Y. Hou, T. Zhang, C. Kuttner, T. Lehnert, G. Seifert, U. Kaiser, A. Fery, Z. K. Zheng and X. L. Feng, *Nat. Commun.*, 2016, **7**, 13461.
- Q. Lu, Y. Yu, Q. Ma, B. Chen and H. Zhang, *Adv. Mater.*, 2016, **28**, 1917-1933.
- C. Tan, X. Cao, X.-J. Wu, Q. He, J. Yang, X. Zhang, J. Chen, W. Zhao, S. Han, G.-H. Nam, M. Sindoro and H. Zhang, *Chem. Rev.*, 2017, **117**, 6225-6331.
- M. A. Lukowski, A. S. Daniel, F. Meng, A. Forticaux, L. Li and S. Jin, *J. Am. Chem. Soc.*, 2013, **135**, 10274-10277.
- Y. Peng, Y. Huang, Y. Zhu, B. Chen, L. Wang, Z. Lai, Z. Zhang, M. Zhao, C. Tan, N. Yang, F. Shao, Y. Han and H. Zhang, *J. Am. Chem. Soc.*, 2017, **139**, 8698-8704.
- N. P. Armitage, J. C. P. Gabriel and G. Gruner, *J. Appl. Phys.*, 2004, **95**, 3228-3230.
- F. C. Krebs, *Energy Mater. Sol. Cells*, 2009, **93**, 394-412.
- H. Sirringhaus, T. Kawase, R. H. Friend, T. Shimoda, M. Inbasekaran, W. Wu and E. P. Woo, *Science*, 2000, **290**, 2123-2126.
- H. Minemawari, T. Yamada, H. Matsui, J. Y. Tsutsumi, S. Haas, R. Chiba, R. Kumai and T. Hasegawa, *Nature*, 2011, **475**, 364-367.
- S. Wang, Q. Wang, P. Shao, Y. Han, X. Gao, L. Ma, S. Yuan, X. Ma, J. Zhou, X. Feng and B. Wang, *J. Am. Chem. Soc.*, 2017, **139**, 4258-4261.
- D. N. Bunck, W. R. Dichtel, *J. Am. Chem. Soc.*, 2013, **135**, 14952-14955.
- S. Chandra, S. Kandambeth, B. P. Biswal, B. Lukose, S. M. Kunjir, M. Chaudhary, R. Babarao, T. Heine and R. Banerjee, *J. Am. Chem. Soc.*, 2013, **135**, 17853-17861.
- S. Mitra, S. Kandambeth, B. P. Biswal, M. A. Khayum, C. K. Choudhury, M. Mehta, G. Kaur, S. Banerjee, A. Prabhune, S. Verma, S. Roy, U. K. Kharu and R. Banerjee, *J. Am. Chem. Soc.*, 2016, **138**, 2823-2828.
- S. Mitra, H. S. Sasmal, T. Kundu, S. Kandambeth, K. Math, D. D. Diaz and R. Banerjee, *J. Am. Chem. Soc.*, 2017, **139**, 4513-4520.
- M. A. Khayum, S. Kandambeth, S. Mitra, S. B. Nair, A. Das, S. S. Nagane, R. Mukherjee and R. Banerjee, *Angew. Chem., Int. Ed.*, 2016, **55**, 15604-15608.
- A. B. Marco, D. Cortizo-Lacalle, I. Perez-Miqueo, G. Valenti, A. Boni, J. Plas, K. Strutynski, S. De Feyter, F. Paolucci, M. Montes, A. N. Khlobystov, M. Melle-Franco and A. Mateo-Alonso, *Angew. Chem., Int. Ed.*, 2017, **56**, 6946-6951.
- W. Liu, Y. Hou, H. Pan, W. Liu, D. Qi, K. Wang, J. Jiang and X. Yao, *J. Mater. Chem. A*, 2018, **6**, 8349-8357.
- Y. Chen, W. Cao, C. Wang, D. Qi, K. Wang and J. Jiang, *Inorg. Chem.*, 2016, **55**, 3151-3160.
- P. Hobza and J. Šponer, *Chem. Rev.*, 1999, **99**, 3247-3276.
- K. Wang, D. Qi, H. Wang, W. Cao, W. Li and J. Jiang, *Chem. Eur. J.*, 2012, **18**, 15948-15952.
- T. D. Thanh, N. D. Chuong, H. V. Hien, T. Kshetri, L. H. Tuan, N. H. Kim and J. H. Lee, *Prog. Mater. Sci.*, 2018, **96**, 51-85.
- Y. Jia, L. Zhang, G. Gao, H. Chen, B. Wang, J. Zhou, M. T. Soo, M. Hong, X. Yan, G. Qian, J. Zou, A. Du and X. Yao, *Adv. Mater.*, 2017, **17**, 1700017.

ARTICLE

Journal Name

- 48 Y. Li, H. Liu, H. Wang, J. Qiu and X. Zhang, *Chem. Sci.*, 2018, **9**, 4132-4141.
- 49 A. B. Soliman, M. H. Hassan, T. N. Huan, A. A. Abugable, W. A. Elmeahmeh, S. G. Karakalos, M. Tsotsalas, M. Heinle, M. Elbahri, M. Fontecave and M. H. Alkordi, *ACS Catalysis*, 2017, **7**, 7847-7854.
- 50 A. B. Soliman, R. R. Haikal, A. A. Abugable, M. H. Hassan, S. G. Karakalos, P. J. Pellechia, H. H. Hassan, M. H. Yacoub and M. H. Alkordi, *ACS Applied Materials & Interfaces*, 2017, **9**, 27918-27926.
- 51 A. B. Soliman, R. R. Haikal, A. A. Abugable and M. H. Alkordi, *J. Mater. Chem. A*, 2017, **5**, 1957-1961.
- 52 A. B. Soliman, M. H. Hassan, A. A. Abugable, S. G. Karakalos and M. H. Alkordi, *ChemCatChem*, 2017, **9**, 2892.
- 53 M. Abel, S. Clair, O. Ourdjini, M. Mossoyan and L. Porte, *J. Am. Chem. Soc.*, 2011, **133**, 1203-1205.
- 54 Z. Honda, Y. Sakaguchi, M. Tashiro, M. Hagiwara, T. Kida, M. Sakai, T. Fukuda and N. Kamata, *Appl. Phys. Lett.*, 2017, **110**, 133101.
- 55 J. P. Perdew, K. Burke and M. Ernzerhof, *Phys. Rev. Lett.*, 1996, **77**, 3865-3868.
- 56 P. J. Hay and W. R. Wadt, *J. Chem. Phys.*, 1985, **82**, 270-283.
- 57 J. S. Binkley, J. A. Pople and W. J. Hehre, *J. Am. Chem. Soc.*, 1980, **102**, 939-947.
- 58 M. J. Frisch, et al. Gaussian 09, Revision D.01. Wallingford, CT: Gaussian Inc. 2013.
- 59 Y. Wang, Y. Lai, L. Song, Z. Zhou, J. Liu, Q. Wang, X. Yang, C. Chen, W. Shi and Y. Zheng, *Angew. Chem., Int. Ed.*, 2015, **54**, 9907-9910.
- 60 K. P. Singh, E. J. Bae and J. Yu, *J. Am. Chem. Soc.*, 2015, **137**, 3165-3168.
- 61 X. Wang, B. Wang, J. Zhong, F. Zhao, N. Han, W. Huang, M. Zeng, J. Fan and Y. Li, *Nano Res.*, 2016, **9**, 1497-1506.
- 62 L. Zhang, J. M. T. A. Fischer, Y. Jia, X. Yan, W. Xu, X. Wang, J. Chen, D. Yang, H. Liu, L. Zhuang, M. Hankel, D. J. Searles, K. Huang, S. Feng, C. L. Brown and X. Yao, *J. Am. Chem. Soc.*, 2018, **140**, 10757-10763.
- 63 U. I. Kramm, I. Herrmann-Geppert, J. Behrends, K. Lips, S. Fiechter and P. Bogdanoff, *J. Am. Chem. Soc.*, 2016, **138**, 635-640.
- 64 L. Zhang, T. Liu, N. Chen, Y. Jia, R. Cai, W. Theis, X. Yang, Y. Xia, D. Yang and X. Yao, *J. Mater. Chem. A*, 2018, **6**, 18417-18425.
- 65 D. Li, Y. Jia, G. Chang, J. Chen, H. Liu, J. Wang, Y. Hu, Y. Xia, D. Yang and X. Yao, *Chem*, 2018, **4**, 2345-2356.
- 66 W. Liu, K. Wang, C. Wang, W. Liu, H. Pan, Y. Xiang, D. Qi and J. Jiang, *J. Mater. Chem. A*, 2018, DOI: 10.1039/c8ta08173e.

View Article Online
DOI: 10.1039/C8TA11044A